J. Phys. B: At. Mol. Opt. Phys. **42** (2009) 154010 (11pp) doi:10.1088/0953-4075/42/15/154010

REVIEW

Experimental and theoretical challenges for the trapped electron quantum computer

I Marzoli[1], P Tombesi[1], G Ciaramicoli[1], G Werth[2], P Bushev[2], S Stahl[2], F Schmidt-Kaler[3], M Hellwig[3], C Henkel[4], G Marx[5], I Jex[6], E Stachowska[7], G Szawiola[7] and A Walaszyk[7]

[1] Dipartimento di Fisica, Università di Camerino, 62032 Camerino, Italy
[2] Department of Physics, Johannes-Gutenberg-University Mainz, 55099 Mainz, Germany
[3] Quanten-Informationsverarbeitung, Universität Ulm, 89069 Ulm, Germany
[4] Institut für Physik und Astronomie, Universität Potsdam, 14476 Potsdam, Germany
[5] Ernst-Moritz-Arndt Universität Greifswald, 17489 Greifswald, Germany
[6] Department of Physics, FJFI ČVUT, 115 19 Praha, Czech Republic
[7] Poznan University of Technology, 60-965 Poznan, Poland

E-mail: irene.marzoli@unicam.it

Received 16 March 2009, in final form 16 April 2009
Published 15 July 2009
Online at stacks.iop.org/JPhysB/42/154010

Abstract
We discuss quantum information processing with trapped electrons. After recalling the operation principle of planar Penning traps, we sketch the experimental conditions to load, cool and detect single electrons. Here we present a detailed investigation of a scalable scheme including feasibility studies and the analysis of all important elements, relevant for the experimental stage. On the theoretical side, we discuss different methods to couple electron qubits. We estimate the relevant qubit coherence times and draw implications for the experimental setting. A critical assessment of quantum information processing with trapped electrons concludes the paper.

(Some figures in this article are in colour only in the electronic version)

1. Introduction

Importance and applications of quantum computing: quantum computers (QC) are known to perform certain computational tasks exponentially more efficiently than their classical counterparts. The theoretical concept of QC [1, 2] is highly developed and especially well known is the algorithm for the factorization of large numbers [3, 4] because it threatens the entire security of commonly used encryption schemes [5, 6]. Furthermore, efficient quantum algorithms exist for searching entries in an unsorted database [7]. More recently, the simulation of quantum spin systems [8–12] has become a focus of research. Worldwide efforts aim at a scalable realization of a QC [13].

Experimental approaches: various schemes have been proposed in the past decade to realize experimentally a first model of a QC and we have seen remarkable experimental and theoretical advances. An overview of experimental techniques towards quantum computing is found in [1, 14–16]. At present, experiments with trapped cold ion crystals confined in linear Paul traps may be regarded as most advanced [17–23]. The main experimental roadblocks are decoherence and scalability. Here we report on recent progress in the experimental and theoretical work with trapped electrons, inspired by the proposal [24], trying to overcome both problems. The idea of using single-electron spins as qubits is also common to other approaches to quantum information, based on semiconductor quantum dots [25, 26]. In our case, however, single electrons

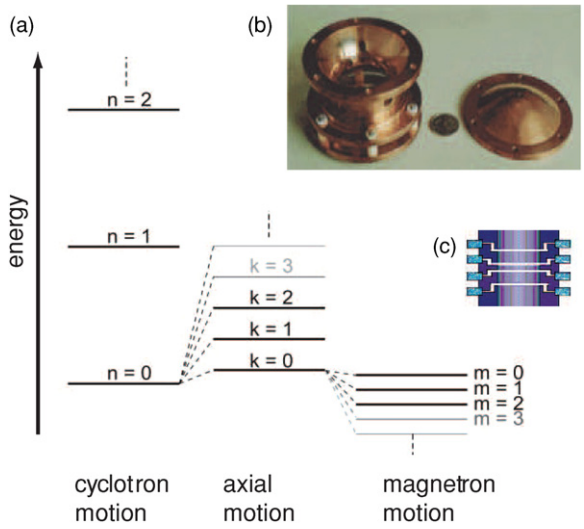

Figure 1. (a) Quantized energy levels of motion for an electron in a Penning trap. (b) Hyperbolic geometry fabricated in copper with cm dimensions for the ideal Penning trap and (c) side view of the design of trap electrodes out of a stack of rings.

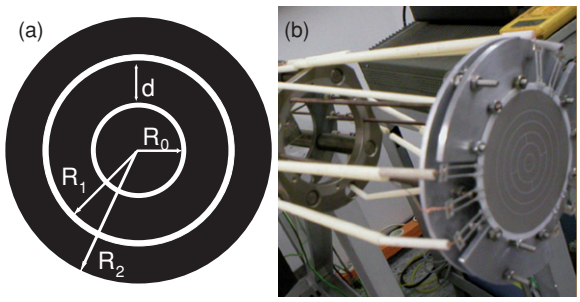

Figure 2. (a) Sketch of a generic planar trap design consisting of a central disk of radius R_0 and a ring electrode of width d and outer radius R_1. A voltage can be applied between the two electrodes while the surface parts outside R_2 are held at ground potential. The electrode with radius R_2 is used to compensate anharmonicities of the potential. (b) Photograph of a prototype planar trap with several ring electrodes surrounding the central disk. The total diameter of the silver plated Al_2O_3 ceramic disk is $D = 48$ mm, with electrodes of $R_0 = 2.5$ mm, $R_1 = 5.8$ mm, $R_2 = 9.1$ mm and $d = 3$ mm. The trap is electrically connected and mounted such that it can be inserted into the magnetic field.

can be trapped in an array of Penning traps at 100 mK. Working in vacuum, without hyperfine interactions with nuclei in the bulk, in a cryogenic environment with only static electric and magnetic fields serves for low decoherence rates. In a two-dimensional array of micro-structured Penning traps each electron stores quantum information in its internal spin and motional degrees of freedom. This architecture allows scalability, similar as in optical lattice experiments but with individual control of qubit sites.

The paper is organized as follows: after introducing the experimental setup of an array of planar Penning traps, we discuss the coupling of two qubits. Taking into account the experimental conditions we estimate single- and two-qubit gate times, and compare these values with the theoretically expected coherence time of electrons in the vicinity of the planar trap electrode. This reasoning allows us to give a critical assessment of the trapped electron approach for a future scalable QC.

2. Penning traps

2.1. Basic properties

The genuine three-dimensional Penning trap [27, 28] is composed of a quadrupole electrical potential Φ^{el} provided by a voltage U applied between a ring electrode and two electrically isolated end cap electrodes of hyperbolic shape (see figure 1(b)), and a superimposed constant magnetic field B_0 in the direction of the z-axis

$$\Phi^{\mathrm{el}}(\rho, z) = \frac{U}{2r_0^2}(\rho^2 - 2z^2). \tag{1}$$

The characteristic dimension of trap electrodes is denoted by r_0. For a properly chosen polarity the electric field serves for confinement between the two end cap electrodes in the axial direction (along the z-axis), while the magnetic field prevents the electrons from escaping in the radial direction ρ. The motion in this potential can be solved analytically and consists of three harmonic oscillations at the frequencies

$$\omega_{\pm} = \left(\omega_{\mathrm{c}} \pm \sqrt{\omega_{\mathrm{c}}^2 - 2\omega_z^2}\right)/2, \tag{2}$$

$$\omega_z = \sqrt{2eU/mr_0^2}, \tag{3}$$

where $\omega_{\mathrm{c}} = eB_0/m$ is the free electron cyclotron frequency, ω_+ is called the reduced cyclotron frequency, ω_- is the magnetron frequency and ω_z is the axial frequency. For our concept these frequencies are of the order of $\omega_+/(2\pi) \sim 100$ GHz, $\omega_-/(2\pi) \sim 10$ kHz, and $\omega_z/(2\pi) \sim 100$ MHz. We note that in the radial direction the electron moves on a potential hill, making the magnetron motion metastable. This also shows up in a diagram of quantized equidistant motional levels, see figure 1(a), where the energy of the magnetron motion decreases with increasing quantum number.

For the electron, the g-factor [29] determines the splitting of spin states via the Larmor frequency $\omega_L = geB_0/2m$ which is slightly above, but well separated from the electron motional frequency component ω_+. Electron spin states are very long lived such that we can identify the qubit computational basis states of the quantum register with the spin states of each electron $\{|0\rangle \equiv |\downarrow\rangle, |1\rangle \equiv |\uparrow\rangle\}_i$ for a collection of N individually trapped single electrons $1 \leqslant i \leqslant N$.

2.2. Planar Penning traps

An application of trapped electrons for QC requires a clear route for the miniaturization of single-electron traps and a design for the multiple interconnections between those individually trapped electrons to allow for quantum gate operations. The planar micro-fabrication technology is well developed and helps designing and fabricating a scalable interconnected multi-trap array. Our approach can be seen in context with other proposals for single ions in linear [10] or two-dimensional [30] arrays of Paul traps, which are possibly

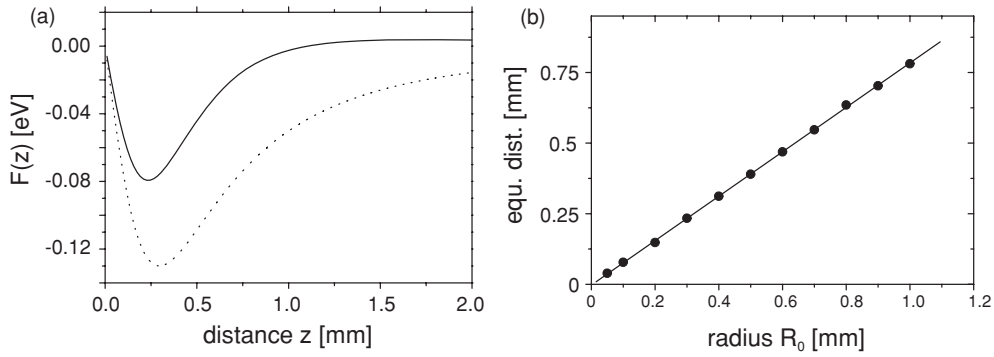

Figure 3. (a) Electric potential $\Phi^{\mathrm{el}}(z)$ for a trap with $R_0 = 300\ \mu$m, $R_1 = 600\ \mu$m, $R_2 = 900\ \mu$m and $U_0 = 0$ V, $U_1 = +0.5$ V, $U_2 = 0$ V leading to a potential with a minimum near $z = 296\ \mu$m and an axial frequency of $\omega_z/(2\pi) = 89.9$ MHz (dashed). Anharmonicities are minimized by changing the compensation voltage to $U_2 = -0.417$ V. The minimum is shifted to a distance of 234 μm for the axial frequency of 99.0 MHz (solid line). (b) Location of the equilibrium position above the surface for the case of a compensated potential. The distance scales linearly as 0.78 R_0.

electrically coupled [31]. The use of a Penning trap with a large planar ion crystal for QC has been discussed in [32].

The basic building block of our approach is a single-electron Penning trap consisting—in its simplest form—of a central disk and a ring electrode on a planar surface, see figure 2(a), where the magnetic field B_0 is perpendicular to the plane. If we apply a voltage between these two electrodes and keep the surrounding parts on ground, the electric potential in the axial direction shows a minimum serving for axial electron confinement.

Harmonic axial potential. The harmonicity of the trap potential is of importance for a number of reasons: particle trapping is more stable and nonlinear resonances [33] are avoided such that a long storage time is guaranteed. Second, the qubit measurement relies on the detection of an inductive voltage pick-up at ω_z from the electron motion which is of the order of a few nV and is therefore detected after a narrowband filtering and amplification, see section 5. Therefore, the signal processing would be difficult, if the motional frequency depended on the axial quantum state k. Third, the cooling of the axial motion, see section 5.1, requires fairly equidistant energy levels.

A particular feature of planar traps is the missing mirror symmetry around the electric potential minimum which makes it impossible to create a perfect harmonic potential in the axial direction. However, as in the case of three-dimensional Penning traps additional electrodes formed out of additional rings serve for partial compensation of anharmonicities. Figure 3(a) shows the calculated potentials with and without compensation. Even though the compensation of higher order coefficients in the Fourier expansion of the potential decreases the depth of the trapping potential, the voltages for trapping are easily increased. Note that with additional electrodes not only the shape of the potential is changed but also the distance of the potential minimum above the surface, see figure 3(b). This will allow us to investigate in detail possible influences of surface effects on the coherence properties of the trapped electrons.

Experimental results from mm-sized planar traps. Operation of two prototype planar traps at room temperature with a total diameter of $D = 48$ mm and 20 mm with clouds of hundreds of electrons shows the expected results [34]: after loading the trap we can excite the different oscillations in axial and radial directions and find agreement with the calculated frequencies. For all details about the operation of this electron trap, the detection of electrons in this setup and the excitation of motional frequencies of the trapped electrons, please see [34]. A planar trap with $D = 20$ mm has been operated at $T = 100$ mK. Clouds of electrons have been stored and detected for 3.5 h, the observed axial frequencies are well understood from calculated potential shapes such as in figure 3(a) [35]. The residual anharmonicity of the axial potential prevented the observation of a single trapped electron. Indeed, analytic calculations and numerical simulations with many ring electrodes show that the frequency broadening, due to the axial anharmonicity, can be reduced, at most, to a few kHz. Unfortunately, this value is still three orders of magnitude larger than the resolution required for single electron detection. A possible way to overcome this problem is the reduction of the trap size to a fraction of a millimetre. The consequent stronger coupling to the external tank circuit, used for the measurement, would allow us to observe a single electron even in the presence of a non-negligible anharmonicity. For this reason we focus on the design and development of smaller traps.

Micro-fabricated single-electron trap with multiple ring electrodes. The design of a micro-fabricated single-electron trap is shown in figure 4(a). Concentrically arranged ring electrodes $E_{1,\ldots,N}$ around a circular central electrode E_0 can be operated as an *effective* circular centre electrode with $U(E_0, E_1, \ldots, E_i) = U_0$ being surrounded by an *effective* ring electrode with $U(E_{i+1}, E_{i+2}, \ldots, E_N) = U_1$ such that the initial trapping volume of the Penning trap is large. After loading the trap using a deep and wide potential, it might be modified adiabatically to reach stiff and harmonic conditions with $U(E_0) = U_0$, $U(E_1) = U_1$, and $U(E_2) = U_2$ serving for the compensation. The distance of the electron to the electrode surface is adjusted by operating the central electrode together with a certain number of rings $E_1, \ldots, E_i$ on the same voltage such that an effective radius R_0 and hereby

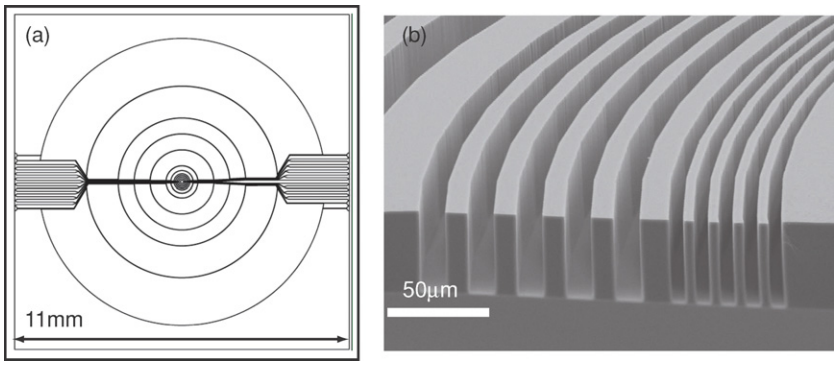

Figure 4. (a) Design of a planar concentric electrode structure for a micro-trap with centre electrode radius that can be varied for a small trap configuration with $R_{0/1/2} = 50/100/150$ μm, intermediate sizes up to a large trap size with $R_{0/1/2} = 1500/3000/4500$ μm. (b) Electron scanning microscope image of a test photo-resist structure with aspect ratio of 5 μm:30 μm before casting with a gold surface.

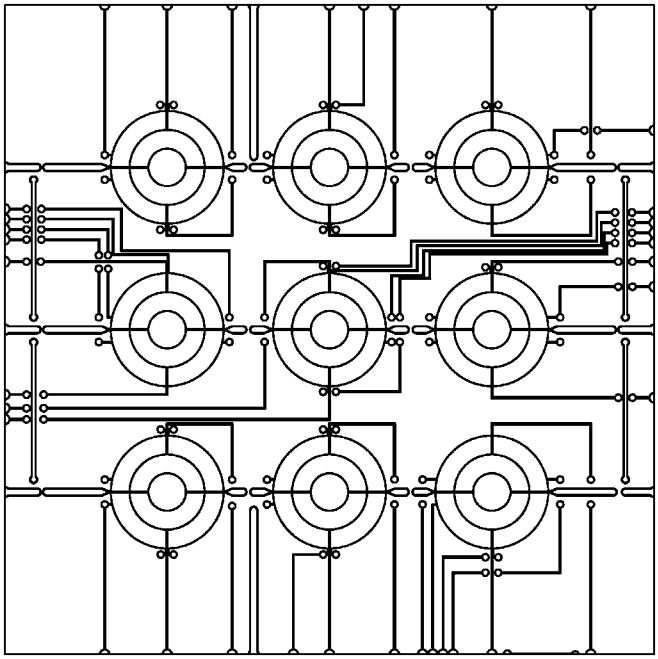

Figure 5. Planar electrode structure for the arrangement of nine interconnected micro-traps of the standard type each with $R_0 = 300$ μm, $R_1 = 600$ μm and $R_2 = 900$ μm. The dimensions correspond to the calculated potential as plotted in figure 3(a). Bonding pads on the gold surface allow for a flexible variation of the connections.

the potential minimum is controlled, see figure 3(b). We refer to section 7 for a detailed discussion of surface decoherence effects that might be investigated by changing the electron–surface distance in a well-determined way.

3. Planar electron trap arrays

For a scalable electron quantum processor the coupling of electrons is important, each of them in its single trap. This coupling is provided by Coulomb interactions, either direct or mediated by wire connections between the micro-traps in the array. The corresponding design is shown in figure 5. It allows connecting the central circular electrode of one of the traps electrically to another one such that the axial motion of electrons might be coupled. With the chip design, the number of mutually coupled traps can be chosen with the gold bonding on the chip such that a number of interconnected qubits is established. Even with a normal conducting wire, coherence is preserved and quantum gates are feasible as discussed in section 6.2.2.

The second approach consists of a planar structure where the voltages on hexagon-shaped electrodes (figure 6) are controlled from outside such that the lateral and vertical positions of the potential minimum of each trap is adjustable. The hexagonal electrode structure allows a freely programmable number of axial potentials. The mutual distance of electrons confined in different potential minima can be reduced such that the direct Coulomb interaction serves for quantum gates. We simulated the potential for a single trap using a self-developed boundary element method [36]. The voltage U_2 for the 12 surrounding hexagons was found that optimizes the harmonicity of the potential, see figure 6(b).

A group at Imperial College London has proposed recently yet another design for planar traps using wires as electrodes [37] and to transport electrons between sites.

4. Overall experimental apparatus

Electrons are loaded from a field emission cathode [38] into the array of planar traps. In general the number of electrons confined in a single planar trap will be larger than one. Excess electrons therefore may be detected and then removed from the trap through the excitation of their axial oscillation by a radio-frequency field, applied to the trap electrodes. The assembly of traps is located at the centre of a superconductive solenoid of $B_0 \sim 3$ T magnetic field strength with the direction perpendicular to the planar surface. The trap is housed in a vacuum container in thermal contact with a dilution refrigerator[8]. At a temperature below 100 mK a vacuum well below 10^{-11} mbar is ensured by cryogenic pumping. The low residual background pressure excludes perturbations by collisions of the electron with residual gas molecules or He atoms for a sufficiently long time. In thermal equilibrium

[8] Oxford Inc., Kelvinox 100.

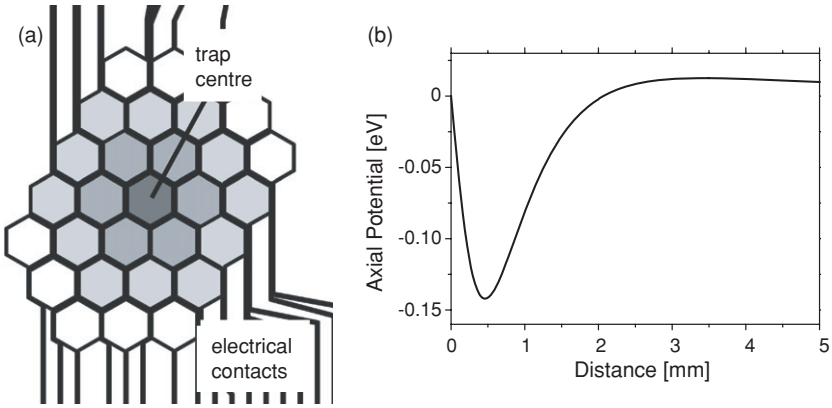

Figure 6. (a) Sketch of the array of 29 planar electrodes, each with a dimension of 0.43 mm, such that all electrodes can be addressed by a different voltage. A trap might be formed above one of the hexagons at $U_0 = 0$ (dark grey in the figure) which is surrounded by six hexagons at $U_1 = +0.6$ V which are again surrounded by 12 hexagons at $U_2 = -0.5015$ V for the compensation of axial anharmonicity. All other electrodes are at $U = 0$ V. (b) The axial potential above the trap centre is obtained by a numerical simulation. We find a trap depth of 0.14 eV in the harmonically compensated potential. A single electron would be trapped at a distance of 0.46 mm with an axial frequency of $\omega_z/(2\pi) = 59.5$ MHz.

with the cold environment the electrons cool into the quantum-mechanical ground-state cyclotron motion by energy loss from synchrotron radiation [39].

The planar trap is equipped with a pick-up coil[9] for the axial motional frequency, followed by an amplifier which sends this rf signal to the outside of the cryostat. A rf signal near ω_z can also be fed-in from an external frequency source for an excitation of the electron. Microwave guides allow sending in frequencies near ω_L or ω_+ serving for the diagnosis and for qubit gate operations. Section 6.1 will describe the required microwave pulses for universal single and two-qubit operations.

5. Electron spin qubit detection

In our setup electrons are detected non-destructively by the induced image charges of the axial motion. The detection provides a direct measurement of

(a) the presence of a single electron or the number of trapped electrons and
(b) the energy of the stored electrons in the axial degree of freedom.

If an inhomogeneous magnetic field B_2 is superimposed on the quantization field B_0 the 'continuous' Stern–Gerlach effect [27, 40–42] allows to

(c) detect the spin state $\{|\uparrow\rangle, |\downarrow\rangle\}$ of the electron and also
(d) the cyclotron motion.

The technically most demanding requirement is a low-noise cryogenic amplification of the ultra-weak inductive pick-up by using a preamplifier at $T = 0.1$ K followed by an amplifier at $T = 0.5$ K [43]. The output signal is detected by a low-noise spectrum analyser[10].

Axial motion detection schemes. To understand the detection method used for (a) and (b), we imagine that the electric *LC* circuit composed by the pick-up coil (a helical copper resonator) and the capacitances from the trap electrodes shows up on the spectrum analyser by the enhancement of noise within a bandwidth that corresponds to the Q-value of the resonance. The values of L and C are chosen such that the resonance is centred at ω_z. Initially, the electrons motional energy in the axial degree of freedom is high and the noise measured by spectrum analyser exceeds the noise background of the naked *LC*-circuit. The coupling to the axial circuit serves for cooling the axial degree of freedom to the environmental temperature ('resistive cooling'). For low electron energy, a dip appears in the noise spectrum, as the motion of the trapped particle 'short-cuts' the *LC*-circuit exactly at the axial trap frequency [41].

The *Stern–Gerlach effect* is understood here as the variation of the axial frequency conditioned on the electron spin state [42, 44]. Any inhomogeneous magnetic field $B_2 \propto z^2$ superimposed on B_0 leads to a coupling of the spin and motional modes of the trapped electron. This inhomogeneity is generated by a ring of ferromagnetic material. The size of the axial frequency shift is controlled by the magnitude of the inhomogeneity, typically a fraction of 10^{-6} of ω_z. As we measure the frequency of the axial dip we can deduce the spin state $\{\downarrow, \uparrow\}$. The method has been applied for the measurement of the magnetic moment of the free and bound electrons [40, 44, 45]. In our proposal, the Stern–Gerlach effect can be dynamically controlled even with constant magnetic fields $B_{0,2}$ by varying the distance of the electron to the surface: the detection of the spin direction should happen at a location close to the central circular trap electrode, e.g., where the inhomogeneity is comparatively large and the pick-off signal for axial detection is relatively high. Further away from the surface, in a more homogeneous field region, the spin state remains undisturbed. The controlled variation of all electron positions also allows for a direct and unambiguous addressability of those qubits by defining their individual Larmor and reduced cyclotron frequencies. For the axial motion the addressing can also be achieved by a slight detuning

[9] Typically connected to the innermost circular electrode.
[10] Signature B, Anritsu Inc., with a displayed average noise floor of −167 dBm.

of the trapping potentials, resulting in different trapping frequencies for every individual electron.

5.1. Sideband cooling and axialization of the electron orbit

To initialize the electrons for quantum gate operations, cooling techniques are employed. As shown by Gabrielse and coworkers [39], the cyclotron energy is quantized and the electron cools by synchrotron radiation to the cryogenic environment, ultimately reaching the ground state $|n = 0\rangle_c$ where it remains if $k_B T \ll \hbar\omega_c$. The same group at Harvard has also demonstrated feedback cooling for the axial oscillator of a trapped electron [46], even though ground-state cooling of the axial degree of freedom is yet to be achieved. Microwave pulses coupling the axial and cyclotron motion $|n = 0\rangle_c|n\rangle_z \rightarrow |n = 1\rangle_c|n-1\rangle_z$ followed by spontaneous decay $|n = 1\rangle_c \rightarrow |n = 0\rangle_c$ will lead to axial cooling [47, 48].

The axialization of the electron motion uses a resonantly driven excitation at the magnetron frequency such that the orbit is stabilized [42, 49, 50].

6. Electron qubit gates

6.1. Single qubit gates

A quite natural choice to encode qubits with trapped electrons is the particle spin. Indeed, the two possible spin orientations $\{|\uparrow\rangle, |\downarrow\rangle\}$ in the trap magnetic field may represent a qubit. Alternatively, the motional degrees of freedom $\{|0\rangle_c, |1\rangle_c\}$ or $\{|0\rangle_z, |1\rangle_z\}$ might serve to encode qubits. Appropriate rf or microwave pulses drive gate operations, addressed to single qubits, while all other qubits stay unperturbed as their frequencies are shifted far from resonance. For the motional qubit states, measures have to be taken not to populate Fock states larger than $|n = 1\rangle$ by composite pulse techniques [22, 51–53], or resorting to anharmonicities [54–56].

6.2. Two-qubit gates

The qubit bases mentioned above allow for various types of conditional qubit dynamics [24, 57]. Here we restrict ourselves to scalable methods and focus on a direct spin–spin interaction mediated by a magnetic field gradient and by an electrical coupling of the electrons axial motion via a direct connection of trap electrodes. While the first one has the advantage of working without ground-state cooling of the axial motion, the second one has the advantage of coupling even distant electron sites in the array.

6.2.1. Effective spin–spin interaction. Consider an array of N electrons that are exposed to an inhomogeneous magnetic field producing a linear gradient $B_1 \propto bx$. This means that the free electron cyclotron frequency ω_c, the spin Larmor frequency ω_L, the reduced cyclotron frequency ω_+ and the magnetron frequency ω_- all depend on the particle position in the array. For instance, with a magnetic gradient of 50 T m^{-1}, the spin flip frequencies of two electrons in neighbouring traps, separated by a distance of the order of 10^{-3} m, differ from each other by a few MHz. This value, though small in comparison with the typical spin frequency $\omega_L/(2\pi) \sim 100$ GHz, is enough to individually address the qubits via microwave radiation. Moreover, the array of traps can accommodate up to tens of qubits, with their frequencies spread over a range of 100 MHz.

Table 1. Coupling strength of the spin–spin interaction J in units $\omega/(2\pi)$ for different values of the magnetic field gradient b and inter-particle distance. The axial frequency $\omega_z/(2\pi)$ is 100 MHz.

	100 μm	50 μm	10 μm
50 T m^{-1}	2.3 Hz	18 Hz	2300 Hz
500 T m^{-1}	0.23 kHz	1.85 kHz	230 kHz

Importantly, the linear magnetic gradient couples the motional degrees of freedom of each particle [58] to its spin state:

$$H_{\text{spin}} = \frac{g}{2}\mu_B \boldsymbol{\sigma} \cdot \mathbf{B}(\mathbf{x}, \mathbf{y}, \mathbf{z}) \tag{4}$$

where μ_B denotes Bohr magneton and σ_x, σ_y and σ_z are Pauli matrices. Moreover, the long-range Coulomb interaction, when treated as a perturbation with respect to the confining potential, establishes a dipole–dipole coupling between the axial motions of the trapped electrons. Thus the application of the magnetic gradient, mediated by the Coulomb repulsion, results in an effective coupling between the spin qubits. As shown in [59], the spin–spin interaction reads

$$H'_{\text{spin-spin}} \simeq \frac{\hbar\pi}{2} \sum_{i>j}^{N} J_{i,j} \;\; \sigma_{z,i} \;\; \sigma_{z,j}. \tag{5}$$

The spin–spin coupling strength $J_{i,j}$ is tunable, since it depends on external parameters like the strength of the applied magnetic field gradient b, the inter-trap distance $d_{i,j}$, and the characteristic trapping frequencies:

$$J_{i,j} = \frac{1}{4\pi\epsilon_0} \frac{g^2\mu_B^2 e^2}{2\pi\hbar m^2} \frac{b^2}{\omega_z^4 d_{i,j}^3}. \tag{6}$$

The Hamiltonian equation (5) is formally analogous to the Hamiltonian describing a system of nuclear spins used to perform NMR quantum computation. This similarity suggests that techniques developed and tested in NMR experiments can be readily exported to trapped electrons in order to implement quantum logic gates. We quote typical orders of magnitude for this spin–spin coupling in table 1.

6.2.2. Coherent wire coupling. We consider next a two-qubit gate implemented with the axial oscillation of two electrons in separate traps that are connected with an 'information exchange wire'. This couples the oscillating image charges on the two electrodes to each other. The case of a superconducting connection [60] was analysed in [61]. We point out here that even with a normally conducting wire, a coherent trap coupling is possible despite the presence of thermal noise. The basic method is a quantum theory of electric signal propagation and noise in resistive circuits at finite temperature [62]. Applying this theory to the two coupled electrons gives (i) a rate $\Omega_{12}/(2\pi)$ for the coherent swapping of excitations between the traps; (ii) dissipation and decoherence rates for both traps, due to the thermal resistance of the wire; and (iii) a

Table 2. Coupling strength of the wire mediated interaction Ω_{12} in units $\omega/(2\pi)$ for different trap radii R_0 and inter-trap distances d. The axial frequency $\omega_z/(2\pi)$ is 100 MHz. According to the results shown in figure 3, h is related to R_0 for a harmonically compensated trap. We assume capacitances $C_0 = R_0 \times 100\,\mathrm{fF\,mm^{-1}}$, $C_\mathrm{w} = d \times 66\,\mathrm{fF\,mm^{-1}}$, realistic for the trap layout of figures 4 and 5.

	$d = 100$ mm	10 mm	1 mm	100 μm	10 μm
$R_0 = 1$ mm	0.12 Hz	1.0 Hz	3.2 Hz	–	–
10 μm	1.3 kHz	13 kHz	130 kHz	990 kHz	3200 kHz

Table 3. Error sources for single-qubit and two-qubit interactions. Axial qubit frequency 100 MHz, cyclotron and spin qubit frequency 100 GHz. The axial qubits are coupled by a gold wire with specifications mentioned after equation (15).

		Electric field	Magnetic field	Axial wire coupling
Relative fluctuation	6×10^{-8} (dc)	$10^{-11}/\sqrt{\mathrm{Hz}}$ @ 1 kHz	$10^{-11}/\sqrt{\mathrm{Hz}}$ @ 1 kHz	Johnson noise @ 100 mK
Decoherence rate	$\sim 10\ \mathrm{s^{-1}}$	$\sim 10^{-5}\ \mathrm{s^{-1}}$	$\sim 10\ \mathrm{s^{-1}}$	$10^{-2}\ \mathrm{s^{-1}}$

dissipative cross-coupling of the electric field fluctuations due to the fact that both traps couple to the same environment.

In the low-frequency regime the wire mainly acts as a capacitive coupler. The coherent coupling is described by the Hamiltonian

$$H_{z,12} = \hbar\Omega_{12}\left(a^\dagger_{z,1}a_{z,2} + a_{z,1}a^\dagger_{z,2}\right), \tag{7}$$

where a and $a^\dagger$ denote the creation and annihilation of axial quanta, and the Rabi frequency [57]

$$\Omega_{12} = \frac{e^2}{2mR_0^2\omega_z}\left(\frac{R_0^2}{h^2+R_0^2}\right)^3\frac{1}{2C_0+C_\mathrm{w}} \tag{8}$$

depends on height of the electron above the trap electrode h and the centre electrode radius R_0. The capacitance $C_0 \sim \pi\varepsilon_0 R_0$ describes the intrinsic electrode capacitance and C_w is the capacitance of the wire connecting the two traps. The shorter the wire (C_w decreases) and the smaller the trap electrodes (R_0 and C_0 decrease), the stronger the coherent coupling [57]. Typical values are quoted in table 2.

The coherent wire coupling could be employed also in the scheme, discussed previously, to establish a stronger spin–spin interaction between distant electrons. Indeed, the effective J coupling results from the interaction of the electrons axial motion. Therefore, the electrical coupling through a wire is especially suitable whenever the Rabi frequency Ω_{12} of equation (8) is much larger than the direct Coulomb repulsion. Hence, the two approaches are not mutually exclusive, but rather complement each other, allowing two-qubit operations to be performed in different regimes.

7. Non-perfect quantum operations

We identify two classes of imperfections which make the trapped electrons lose their ability to persist in certain quantum superposition states. An obvious source of dephasing is fluctuations in the control parameters for a quantum operation such as the trap dc voltages, magnetic field stability or microwave frequency and phase. Table 3 lists several of the effects for typical parameters in the experiment. A second class of decoherence arises from more fundamental couplings where the fluctuations are of quantum or thermal origin, typical examples are the spontaneous decay of the cyclotron Fock states or the Johnson noise in a metallic conducting surface which couples to the axial motional degree of the electron.

7.1. Fluctuating control parameters

The noise from fluctuations of the *trap control voltages* has been estimated as follows: the 24 bit voltage supply allows a stability of $\Delta U/U \simeq 6 \times 10^{-8}$. This translates into (quasi-static) fluctuations of the axial trapping frequency, $\Delta\omega_z/\omega_z = \frac{1}{2}\Delta U/U$. A characteristic dephasing time τ_z for superposition states of the axial qubit can be defined by $\Delta\omega_z\tau_z \sim 1$. For the axial frequency of 100 MHz mentioned above, this gives $\tau_z \sim 50$ ms. These fluctuations can be compared to dynamical noise that leads to a diffusive increase of the relative phase at the rate $\gamma_z \sim (\omega_z/2)^2 S_U/U^2$, where S_U is the power spectral density of the voltage noise. (We normalize S_U such that the rms voltage noise δU in a frequency band $\Delta\nu$ is $(2S_U\Delta\nu)^{1/2}$.) The same reasoning applies to the dephasing of the cyclotron and spin qubits where the relative phase of superposition states is randomized by magnetic field fluctuations. Values that we estimate as realistic for the cryogenic electronics used in our experiments are collected in table 3 and show that the limiting factors are dc electric field stability (for the axial qubit) and magnetic field fluctuations (for the cyclotron qubit).

To obtain a well-defined control of the qubit states, external rf and microwave fields are required and their amplitude and phase uncertainties have to be considered. Fortunately one benefits here from the cryogenic environment and the fact that the excitation signals can be created by nonlinear effects directly in the cold region. Hence in the 'off' state, when the drives are not active, the externally introduced additional noise background is negligible. The remaining noise from the trap environment can be estimated as described in section 7.2, concerning the cyclotron and spin transitions. When the drives for manipulating the quantum states (axial, cyclotron or spin) are turned 'on', their amplitude and phase uncertainties within the respective excitation times come into play. It is expected that the respective rf and microwave signals, while guided from the room temperature region into the cryogenic trap setup, do not suffer considerable short-term amplitude or phase variations. Therefore, the same considerations as for comparable room temperature setups and the manipulation of qubits in trapped ions can be applied [20, 28, 51]. However, taking into account manipulation rates of qubit states not faster than a few kHz, it can be expected that the latter effects are rather small compared to all other decoherence mechanisms.

7.2. Thermal and quantum noise from the trap environment

The *cyclotron oscillation* is driven towards its ground state via electric dipole coupling to electric vacuum fluctuations. This happens, in free space, at the spontaneous emission rate

$$\gamma_c = \frac{e^2\omega_+^2}{3\pi\varepsilon_0 mc^3} \tag{9}$$

corresponding to a decay time of a few seconds. Thermal fluctuations can be ignored since at 100 mK, the occupation numbers of states with one or more photons (energy $\hbar\omega_+$) are negligible. In our apparatus with a half-open geometry, standing waves may form (cyclotron wavelength of 3.0 mm at 100 GHz) such that the spontaneous emission rate is slightly modified [27].

The *spin state* of the trapped electrons suffers heating and decoherence from magnetic field fluctuations. If we follow the master equation approach outlined in [56], the dynamics of the relevant matrix elements of the spin density operator ρ^{spin} is given by

$$\dot{\rho}_{\downarrow\downarrow} = -2\Gamma_-\rho_{\downarrow\downarrow} + 2\Gamma_+\rho_{\uparrow\uparrow}, \tag{10}$$

$$\dot{\rho}_{\downarrow\uparrow} = \mathrm{i}\omega_L\rho_{\downarrow\uparrow} - 3(\Gamma_- + \Gamma_+)\rho_{\downarrow\uparrow}. \tag{11}$$

Unintended spin flips $|\downarrow\rangle \to |\uparrow\rangle$ ($|\uparrow\rangle \to |\downarrow\rangle$) take place with a rate $2\Gamma_-$ ($2\Gamma_+$), while the coherence decays with a rate $3(\Gamma_- + \Gamma_+)$. The rates

$$\Gamma_\pm \equiv \left(\frac{ge}{4m}\right)^2 S_B(\pm\omega_L) \tag{12}$$

depend on the spectral density $S_B(\omega)$ of the magnetic field fluctuations at the Larmor frequency,

$$S_B(\omega) = \int_{-\infty}^{\infty} \mathrm{d}t\, \mathrm{e}^{-\mathrm{i}\omega t}\langle B_z(t)B_z(0)\rangle. \tag{13}$$

In the strong magnetic fields and low temperatures considered here, this spectrum is dominated by vacuum fluctuations, as for the cyclotron oscillation, and modified by the trap geometry. Relative to the cyclotron decay rate (9), spin decay is suppressed by a factor $\hbar\omega_L/mc^2 \sim 10^{-9}$ and hence negligible. Low frequency fluctuations make the phase of $\rho_{\downarrow\uparrow}$ drift, limiting the phase coherence as discussed in section 7.1.

The *axial qubit* has a level spacing small compared with the environmental energy $\hbar\omega_z \ll k_B T$ such that this oscillator ends in a thermal state $n_z \gg 1$. However, the electron can be driven to the axial ground state using sideband-cooling techniques as mentioned in section 5.1. Once the axial oscillator is prepared in its vibrational ground state, the coupling to quasi-static electric field fluctuations from charges and currents in the circuitry surrounding the trap becomes important. The relevant quantity is the spectral power $S_E(\omega_z)$ of the electric field fluctuations E_z at the axial frequency, defined by analogy to equation (13). This leads to a heating rate:

$$\gamma_z = \frac{e^2}{2\hbar m\omega_z} S_E(\omega_z). \tag{14}$$

Heating also destroys superposition states and limits the coherence time for the axial qubit. Electric noise is generated from several sources, such as patch charge fluctuations and thermal Johnson noise from the detection circuit. Noise inherent to the electrode material turns out to amount to a negligible heating rate. Additionally, the fluctuations of the trap control voltages contribute significantly to the axial dephasing rate. They have been estimated in section 7.1.

The heating due to *patch charge fluctuations* has been observed in radio-frequency ion traps with sub-mm sizes [63, 64]. The heating rate decreases strongly for a temperature of 4 K [65]. Compared to the Paul traps for ions, our experiment is operated at a temperature which is two orders of magnitude lower and the static dc voltages for the electron confinement are not driving the motion of patches. We have extrapolated the electric field noise from ion trap measurements [65] to our setup and expect a very low heating and decoherence rate from this noise source. The contribution of charge fluctuations on the dielectric parts of the circuit board is likely to be weak given that most of the board is metallized. On the other hand, the experiment with trapped electrons may help in understanding the physical mechanism behind these phenomena.

Even if the electrode surfaces are prepared in an ideal way that a purely metallic conducting surface without any surface contaminations is facing the trapped electrons, the *intrinsic damping properties* of the material will lead to noise. The corresponding heating rate increases with the ac resistivity of the electrode material and with the electrode temperature, and decreases with the axial frequency and distance h. For gold electrodes with a radius of 100 μm we expect a rate of $\gamma_z \simeq 10^{-3}$ s^{-1} [66].

Johnson noise from attached circuitry plays a role only during the instance of qubit measurement. During single-qubit gate operations, the electrons are decoupled from the circuit. If we work with the direct spin–spin coupling two qubit interaction, see section 6.2.1, also no circuit is attached and the gate is not affected by this noise source. If for some reason, the measurement circuit needs to be constantly kept resonant to the electron axial motion, any resistive element in this circuitry generates Johnson–Nyquist voltage noise with a spectrum $S_V(\omega) = 2\, k_B T\, R_c(\omega)$. This expression applies in the low frequency regime, $\hbar\omega_z \ll k_B T$. The voltage noise is filtered by the circuit, in particular capacitances, before arriving at the trap electrode [67]. For a temperature of 100 mK, a circuit impedance of 100 kΩ, a quality factor of 10^3 and a trap central electrode radius of 100 μm we estimate $\gamma_z \simeq 10$ s^{-1} (see table 3).

Johnson voltage noise also affects the wire coupling of two qubits. Here the dissipation stems from the finite resistance of the coupling wire. To illustrate the impact of decoherence on the two-qubit wire gate, we consider the SWAP operation. The axial qubits are initialized in the state $|n_1 = 1, n_2 = 0\rangle$, and the coherent coupling via the wire is switched on for a time $\tau = \pi/\Omega_{12}$. After this time, the excitation of qubit 1 should have been transferred to qubit 2 resulting in the state $|n_1 = 0, n_2 = 1\rangle$. Due to the thermal fluctuations in the wire, this state is only reached with a reduced fidelity. The relevant figure of merit for this two-electron scheme is the maximum

number of gate operations $N_{\max}$ that are possible within a decoherence time [57]:

$$N_{\max} \approx \frac{\Omega_{12}}{\pi \gamma_z} \approx \frac{3\hbar}{4\pi k_B T R_w (2C_0 + C_w)}. \quad (15)$$

Realistic parameters for a gold wire of 20 μm diameter and 150 μm length are $C_0 \simeq C_w \simeq 10$ fF, $R_w \simeq 1$ mΩ, noting that the axial coupling occurs in a frequency range where radiative impedances are negligible. We also neglect resistive losses across the dielectric substrate the wire is deposited on. This gives $N_{\max} > 10^5$ at 100 mK.

8. Conclusion

Certainly the various experimental techniques for QC show different assets and difficulties. At the current status of research we summarize the assets of our proposal along the criteria as formulated by DiVincenzo [68].

Absolutely mandatory is the scalability of the approach that should at least allow scaling to the order of 100 qubits. The dimensionality of the technique will determine how efficient algorithms may be executed. Examples are the one-dimensional techniques such as linear cold ion crystals, but also two-dimensional geometries which are for example realized in circuits of superconducting elements on a planar substrate. An example of a three-dimensional system is an optical lattice formed by three laser fields and holding cold atoms at the lattice sites. Our electron trap array combines a two-dimensional geometry with individual control over every qubit site. The size of micro-Penning traps will allow a high number of qubit sites on a single chip.

Coherence times are expected to be very long, due to the reduced noise in a cryogenic and well-shielded environment. The purely static control voltages improve further the coherence properties.

Gate operation times for single- and two-qubit operations should be much shorter than the decoherence time. According to our estimations this is largely fulfilled. All gate operations can be implemented with standard radio frequency and microwave equipment, which commercially delivers low phase noise. The gates which we described can be operated highly parallel, e.g. the electrically conducting wire may serve as a quantum bus allowing interactions between any pair of qubits in the register, not only between two nearest neighbours. To this end, we plan to develop and operate an array of sub-millimetre sized interconnected planar traps. The smaller size should also help in detecting a single trapped electron, even in the presence of some residual anharmonicity in the axial potential.

In our quantum register, qubits are read out with the help of the Stern–Gerlach effect which has already been used for decades in precision spectroscopy with trapped electrons. The scheme allows even for a parallel read-out. For the initialization of spin state we rely on a non-destructive measurement, while the motional qubits degrees are laserless cooled.

Finally, the future QC may benefit from a combination and connectivity of different techniques, in a similar way as our conventional computer uses a magnetic storage device and an electronic processor from semiconductor materials, both connected by normal conducting metal leads. Therefore it is of high importance that qubit information may be transferred via electrically conducting wires. The low temperature surface forming the single-electron Penning traps may allow for an integration of and coupling to superconducting circuit elements for QC.

In view of realizing quantum phase transitions one might think of grouping the qubit sites, e.g. building linear or ring structures with either even or odd numbers of sites, forming two-dimensional lattices with or without frustration or configurations of the Kagomé type [69]. This would allow simulating interacting spin systems with highly variable and designable properties.

Acknowledgment

We acknowledge financial support by the European Union within the sixth framework programme (contract no. FP6-003772).

References

[1] Nielsen M A and Chuang I L 2000 *Quantum Computation and Quantum Information* (Cambridge: Cambridge University Press)
[2] Mermin N D 2007 *Quantum Computer Science* (Cambridge: Cambridge University Press)
[3] Shor P W 1994 Algorithms for quantum computation: discrete logarithms and factoring *Proc. 35th Ann. Symp. Foundations of Computer Science* ed S Goldwasser (New York: IEEE Computer Society Press) p 124
[4] Ekert A and Jozsa R 1996 Quantum computation and Shor's factoring algorithm *Rev. Mod. Phys.* **68** 733
[5] http://mathworld.wolfram.com/news/2005-11-08/rsa-640/
[6] Rivest R L, Shamir A and Adelman L 1977 On digital signatures and public key cryptosystems *MIT Laboratory for Computer Science Technical Memorandum* 82
[7] Grover L K 1997 Quantum computers can search arbitrarily large databases by a single query *Phys. Rev. Lett.* **79** 325
[8] Lloyd S 1996 Universal quantum simulators *Science* **273** 1073
[9] Jané E, Vidal G, Dür W, Zoller P and Cirac J I 2003 Simulation of quantum dynamics with quantum optical systems *Quantum Inf. Comput.* **3** 15
[10] Deng X-L, Porras D and Cirac J I 2005 Effective spin quantum phases in systems of trapped ions *Phys. Rev.* A **72** 063407
[11] Porras D and Cirac J I 2004 Effective quantum spin systems with trapped ions *Phys. Rev. Lett.* **92** 207901
[12] Ciaramicoli G, Marzoli I and Tombesi P 2008 Quantum spin models with electrons in Penning traps *Phys. Rev.* A **78** 012338
[13] The roadmap of the US and a strategic report of the EU are found, respectively, at http://qist.lanl.gov/ and http://qist.ect.it/
[14] Bruss D and Leuchs G (ed) 2006 *Lectures on Quantum Information* (New York: Wiley)
[15] Bouwmeester D, Ekert A and Zeilinger A (ed) 2006 *The Physics of Quantum Information* (Heidelberg: Springer)
[16] Chen G, Church D A, Englert B-G, Henkel C, Rohwedder B, Scully M O and Zubairy M S 2006 *Quantum Computing Devices: Principles, Designs, and Analysis* (London: Chapman and Hall)
[17] Cirac J I and Zoller P 1995 Quantum computations with cold trapped ions *Phys. Rev. Lett.* **74** 4091–4

[18] Häffner H *et al* 2005 Scalable multiparticle entanglement of trapped ions *Nature* **438** 643–6

[19] Leibfried D *et al* 2005 Creation of a six-atom "Schrödinger cat" state *Nature* **483** 639–42

[20] Leibfried D *et al* 2003 Experimental demonstration of a robust, high-fidelity geometric two ion-qubit phase gate *Nature* **422** 412

[21] Schmidt-Kaler F *et al* 2003 How to realize a universal quantum gate with trapped ions *Appl. Phys.* B **77** 789

[22] Schmidt-Kaler F, Häffner H, Riebe M, Gulde S, Lancaster G P T, Deuschle T, Becher C, Roos C F, Eschner J and Blatt R 2003 Realization of the Cirac–Zoller controlled-NOT quantum gate *Nature* **422** 408

[23] Wineland D J *et al* 2003 Quantum information processing with trapped ions *Phil. Trans. R. Soc. Lond.* A **361** 1349–61

[24] Ciaramicoli G, Marzoli I and Tombesi P 2003 Scalable quantum processor with trapped electrons *Phys. Rev. Lett.* **91** 017901

[25] Loss D and DiVincenzo D P 1998 Quantum computation with quantum dots *Phys. Rev.* A **57** 120

[26] Hanson R, Kouwenhoven L P, Petta J R, Tarucha S and Vandersypen L M K 2007 Spins in few-electron quantum dots *Rev. Mod. Phys.* **79** 1217

[27] Brown L S and Gabrielse G 1986 Geonium theory: physics of a single electron or ion in a Penning trap *Rev. Mod. Phys.* **58** 233–311

[28] Major F G, Gheorge V and Werth G 2006 *Charged Particle Traps* (Heidelberg: Springer)

[29] Hanneke D, Fogwell S and Gabrielse G 2008 New measurement of the electron magnetic moment and the fine structure constant *Phys. Rev. Lett.* **100** 120801

[30] Chiaverini J and Lybarger W E 2008 Laserless trapped-ion quantum simulations without spontaneous scattering using microtrap arrays *Phys. Rev.* A **77** 022324

[31] Häffner H private communication

[32] Porras D and Cirac J I 2006 Quantum manipulation of trapped ions in two dimensional Coulomb crystals *Phys. Rev. Lett.* **96** 250501

[33] Alheit R, Enders K and Werth G 1995 Isotope separation by nonlinear resonances in a Paul trap *Appl. Phys.* B **62** 511

[34] Galve F and Werth G 2006 *Proc. 2006 Non-Neutral Plasma Workshop (Aarhus)*

[35] Bushev P, Stahl S, Natali R, Marx G, Stachowska E, Werth G, Hellwig M and Schmidt-Kaler F 2008 Electrons in a cryogenic planar Penning trap and experimental challenges for quantum processing *Eur. Phys. J.* D **50** 97–102

[36] Schulz S, Poschinger U, Singer K and Schmidt-Kaler F 2006 Optimization of segmented linear Paul traps and transport of stored particles *Fortschr. Phys.* **54** 648–65

[37] Castrejon-Pita J R and Thompson R C 2005 Proposal for a planar Penning ion trap *Phys. Rev.* A **72** 013405

[38] Stahl S, Galve F, Alonso J, Djekic S, Quint W, Valenzuela T, Verdu J, Vogel M and Werth G 2005 A planar Penning trap *Eur. Phys. J.* D **32** 139

[39] Peil S and Gabrielse G 1999 Observing the quantum limit of an electron cyclotron: QND measurements of quantum jumps between Fock states *Phys. Rev. Lett.* **83** 1287–90

[40] Van Dyck R S, Schwinberg P B and Dehmelt H G 1987 New high-precision comparison of electron and positron g factors *Phys. Rev. Lett.* **59** 26–9

[41] Diederich M, Häffner H, Hermannspahn N, Immel M, Kluge K J, Ley R, Mann R, Quint W, Stahl S and Werth G 1998 Observing a single hydrogen-like ion *Hyperfine Interact.* **115** 185

[42] Dehmelt H 1986 Continuous Stern Gerlach effect: principle and idealized apparatus *Proc. Natl Acad. Sci. USA* **53** 2291

[43] Peil S E 1999 Quantum jumps between Fock states of an ultracold electron cyclotron oscillator *PhD Thesis* unpublished, Harvard University, Cambridge, MA

[44] Werth G, Häffner H and Quint W 2002 The continuous Stern–Gerlach effect on atomic ions *Adv. At. Mol. Opt. Phys.* **48** 191

[45] Odom B, Hanneke D, D'Urso B and Gabrielse G 2006 New measurement of the electron magnetic moment using a one-electron quantum cyclotron *Phys. Rev. Lett.* **97** 030801

[46] D'Urso B, Odom B and Gabrielse G 2003 Feedback cooling of one-electron oscillator *Phys. Rev. Lett.* **90** 043001

[47] Cornell E A, Weisskoff R M, Boyce K R and Pritchard D E 1990 Mode coupling in a Penning trap: π pulses and a classical avoided crossing *Phys. Rev.* A **41** 312–5

[48] Verdu J L, Djekic S, Valenzuela T, Häffner H, Quint W, Kluge H J and Werth G 2002 Measurement of the g_j factor of a bound electron in hydrogen-like oxygen $^{16}O^{7+}$ *Can. J. Phys.* **80** 1233–40

[49] Schweikhard L and Marshall A G 1993 Excitation modes for Fourier transform ion cyclotron resonance mass spectrometry *J. Am. Soc. Mass Spectrom.* **4** 433

[50] Powell H F, Segal D M and Thompson R C 2002 Axialization of laser cooled magnesium ions in a Penning trap *Phys. Rev. Lett.* **89** 0930031

[51] Gulde S, Riebe M, Lancaster G P T, Becher C, Eschner J, Häffner H, Schmidt-Kaler F, Chuang I L and Blatt R 2003 Implementing the Deutsch–Jozsa algorithm on an ion-trap quantum computer *Nature* **421** 48

[52] Childs A M and Chuang I M 2001 Universal quantum computation with two-level trapped ions *Phys. Rev.* A **63** 012306

[53] Stortini S and Marzoli I 2005 Composite pulses for quantum computation with trapped electrons *Eur. Phys. J.* D **32** 209

[54] Ciaramicoli G, Marzoli I and Tombesi P 2001 Realization of a quantum algorithm using a trapped electron *Phys. Rev.* A **63** 052307

[55] Ciaramicoli G, Marzoli I and Tombesi P 2002 Three-qubit network with a single trapped electron *J. Mod. Opt.* **49** 1307

[56] Ciaramicoli G, Marzoli I and Tombesi P 2004 Trapped electrons in vacuum for a scalable quantum processor *Phys. Rev.* A **70** 032301

[57] Zurita-Sánchez J R and Henkel C 2008 Wiring up single electron traps to perform quantum gates *New J. Phys.* **10** 083021

[58] Mintert F and Wunderlich Ch 2001 Ion-trap quantum logic using long-wavelength radiation *Phys. Rev. Lett.* **87** 257904

[59] Ciaramicoli G, Galve F, Marzoli I and Tombesi P 2005 Array of planar Penning traps as a nuclear magnetic resonance molecule for quantum computation *Phys. Rev.* A **72** 042323

[60] Majer J *et al* 2007 Coupling superconducting qubits via a cavity bus *Nature* **449** 443

[61] Sørensen A S, van der Wal C H, Childress L I and Lukin M D 2004 Capacitive coupling of atomic systems to mesoscopic conductors *Phys. Rev. Lett.* **92** 063601

[62] Zurita-Sánchez J R and Henkel C 2006 Lossy electrical transmission lines: thermal fluctuations and quantization *Phys. Rev.* A **73** 063825

[63] Schulz S, Poschinger U, Ziesel F and Schmidt-Kaler F 2008 Sideband cooling and coherent dynamics in a microchip multi-segmented ion trap *New J. Phys.* **10** 045007

[64] Epstein R J *et al* 2007 Simplified motional heating rate measurements of trapped ions *Phys. Rev.* A **76** 033411

[65] Labaziewicz J, Ge Y, Antohi P, Leibrandt D, Brown K R and Chuang I L 2008 Suppression of heating rates in

cryogenic surface-electrode ion traps *Phys. Rev. Lett.* **100** 013001

[66] Henkel C, Pötting S and Wilkens M 1999 Loss and heating of particles in small and noisy traps *Appl. Phys.* B **69** 379–87

[67] Deslauriers L, Olmschenk S, Stick D, Hensinger W K, Sterk J and Monroe C 2006 Scaling and suppression of anomalous quantum decoherence in ion traps *Phys. Rev. Lett.* **97** 103007

[68] DiVincenzo D P 2001 Dogma and heresy in quantum computing *Quantum Inf. Comput.* **1** 1

[69] Damski B, Everts H-U, Honecker A, Fehrmann H, Santos L and Lewenstein M 2005 Atomic Fermi gas in the trimerized Kagomé lattice at $2/3$ filling *Phys. Rev. Lett.* **95** 060403